

Local resistance switching at grain and grain boundary surfaces of polycrystalline tungsten oxide films

This article has been downloaded from IOPscience. Please scroll down to see the full text article.

2011 Nanotechnology 22 254008

(<http://iopscience.iop.org/0957-4484/22/25/254008>)

View [the table of contents for this issue](#), or go to the [journal homepage](#) for more

Download details:

IP Address: 159.226.35.189

The article was downloaded on 17/05/2011 at 05:25

Please note that [terms and conditions apply](#).

Local resistance switching at grain and grain boundary surfaces of polycrystalline tungsten oxide films

Da-Shan Shang, Lei Shi, Ji-Rong Sun and Bao-Gen Shen

Beijing National Laboratory for Condensed Matter Physics and Institute of Physics,
Chinese Academy of Sciences, Beijing 100190, People's Republic of China

E-mail: shang_da_shan@163.com

Received 14 August 2010, in final form 31 October 2010

Published 16 May 2011

Online at stacks.iop.org/Nano/22/254008

Abstract

Resistance switching behavior has been investigated in as-prepared and oxygen-annealed polycrystalline tungsten oxide films using conductive atomic force microscopy. The oxygen-annealed film appeared more insulative than the as-prepared films. The local current distributions demonstrated the lower conductivity at the grain boundaries than at the grains in the oxygen-annealed films. Reversible resistance switching behavior only occurred at the grain surface region of the oxygen-annealed films and the resistance switching process was described by the local valence change of tungsten ions induced by electrochemical migration of protons or oxygen vacancies. This different resistance switching behavior between the grain and grain boundary surface was attributed to the different oxygen vacancy density caused by the post-annealing process. The present results would be especially meaningful for the fabrication of nanoscale resistive nonvolatile memory devices.

(Some figures in this article are in colour only in the electronic version)

1. Introduction

One of the most promising candidates for next-generation nonvolatile memory involves a two-terminal resistance device, called resistance random access memory (RRAM) [1–10]. The nonvolatile memory effect of RRAM comes from the reversible resistance switching of the devices between a high resistance state (HRS) and a low resistance state (LRS) by external electrical triggering. A large variety of materials have been found to show this nonvolatile memory effect, including perovskite oxides [1–3], binary transition-metal oxides [4–7] and solid electrolytes [8–10]. There is increasing evidence that the resistance switching can take place at a region with very little area [11–15]. This feature imbues RRAM with a competitive potential to fabricate nonvolatile memory with high scalability. In fact, most of the materials exhibit resistance switching in the polycrystalline structure, in which grains pack together and separate by grain boundaries. As the dimensions of individual elements in devices continue to shrink, especially as the elements approach the level of size comparable to the individual grains of the polycrystalline film,

such grain boundary effects on the resistance switching will become more technologically important. However, little is currently known about the resistance switching properties at individual grains and grain boundaries, since conventional macroscopic measurements are integrated over a fairly large area and cannot spatially resolve the highly local properties. Conductive atomic force microscopy (CAFM) has proven to be an effective method for the investigation of the local electricity of transition-metal oxides, since the conductive tip has lower area than the grain size and can serve as one of the electrodes of the devices [11–19]. The main purpose of this study was to examine the resistance switching at the grain surface (GS) and grain boundary surface (GBS) of polycrystalline tungsten oxide using the CAFM method.

2. Experiment

Commercial glass sputtered with a ~150 nm thick fluorine-doped tin oxide (FTO) thin film was used as both the bottom electrode and substrate. A tungsten oxide ceramic with the nominal composition of WO_3 was used as the target. WO_3

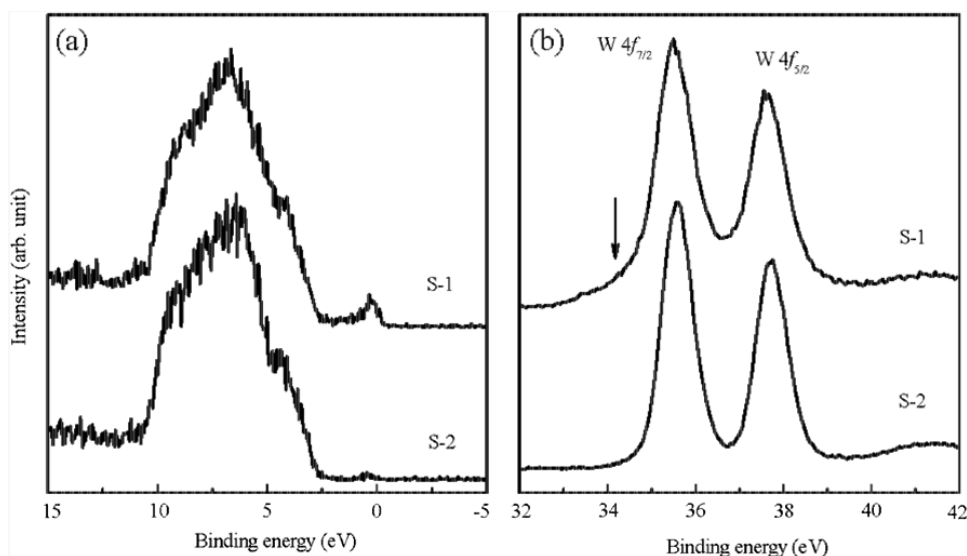


Figure 1. Valence band (a) and W 4f core level (b) spectra of the S-1 and S-2 samples.

films, ~ 400 nm in thickness, were deposited on the substrates by the pulsed-laser ablation technique, with a laser wavelength of 248 nm (KrF excimer laser), a repetition rate of 5 Hz and a fluence of 7 J cm^{-2} . The substrate temperature was kept at 400°C and the oxygen pressure at 10 Pa. After deposition, the film was *in situ* annealed at 400°C for 30 min under an oxygen pressure of 0.1 MPa, then cooled down to room temperature. The resultant samples were denoted as S-2, while the films without post-annealing were denoted as S-1. The oxidation state of the S-1 and S-2 samples were analyzed by x-ray photoemission spectroscopy (AXIS Ultra DLD, Shimadzu Corporation) with a monochromatic Al $K\alpha$ line. The CAFM mode of a scanning probe microscope (Seiko Instruments, SPA400) with an Rh-coated Si tip (the nominal tip diameter is ~ 25 nm), which was grounded, was used for the investigation of the local electrical property of the samples.

3. Results and discussion

Figures 1(a) and (b) show the valence band and W 4f core level spectra, respectively. The valence band spectrum of the S-1 (top curve) shows two main peaks. The first one between 2.5 and 10 eV arises from the O 2p and W 5d states, and the second one, which is close to the Fermi level, is associated with the W 5d states [20]. As is well known, there is no electronic state near the Fermi level in stoichiometric WO_3 [20]. The electronic states near the Fermi level in S-1 could be a signature of the deviation of the oxygen content from the stoichiometric value. Oxygen annealing improved the oxygen stoichiometry of the sample, thus causing a density reduction of this state, as demonstrated by the data of S-2. This is in agreement with the change of the W 4f core level spectra. As shown in figure 1(b), the W 4f core level spectrum consists of the W $4f_{7/2}$ and W $4f_{5/2}$ doublet peaks, with the spin-orbit splitting energy of 2.1 eV [21]. However, an evident shoulder at the low energy side of the W $4f_{7/2}$ peak can be seen in the S-1 sample (arrowed in figure 1(b)), due to the presence of W^{5+} [22]. This feature is

not obvious in S-2, which suggests a reduction of the density of the W^{5+} states after oxygen annealing.

Figure 2 shows the topography and the corresponding current images of the samples under a tip bias of 0.5 V. Both S-1 and S-2 films have polycrystalline structure with a grain size of 100–150 nm (figures 2(a) and (c)). However, the electric property is significantly different. The corresponding current of S-1 reached the current compliance (100 pA) almost in the whole area measured, implying a good conductance. In contrast, a much lower current, below 1 pA, was obtained for S-2, implying an insulative character. Considering the added annealing process for S-2, we suggest that the distinctly different conductivity between S-1 and S-2 should be mainly caused by the concentration of non-stoichiometric defects, such as oxygen vacancies, which introduce donor levels into the bandgap, thus yielding extra carriers from these donor levels [23]. The oxygen-annealing process would reduce the concentration of the oxygen vacancy in the films and thus the film conductivity, as occurred in S-2.

The conductivity of S-2 was further investigated by changing the tip bias in the sequence of $1.0 \text{ V} \rightarrow 1.5 \text{ V} \rightarrow 2.0 \text{ V} \rightarrow -1.0 \text{ V} \rightarrow -1.5 \text{ V} \rightarrow -2.0 \text{ V}$ during scanning the same area as in figure 2(c). When the tip bias came to 1.0 V and then 1.5 V, some of the regions, corresponding to the GS, became conductive, while the regions corresponding to the GBS were still insulative (see figures 3(a) and (b)). This trend became more obvious as the tip bias reached 2.0 V (see figure 3(c)). Since the S-1 and S-2 samples have similar surface morphologies but show a very different conductivity pattern, the possibility of a tip-induced measurement artifact can be ruled out. From the current distribution, it can be concluded that the GS could be more conductive than the GBS. This conclusion was further confirmed by the results obtained under the negative tip bias of -1.0 and -1.5 V (see figures 2(d) and (e)). Different from applying a 2.0 V bias, however, the GBS also became conductive when the tip bias reached -2.0 V (see figure 3(f)), implying an asymmetric current transport at

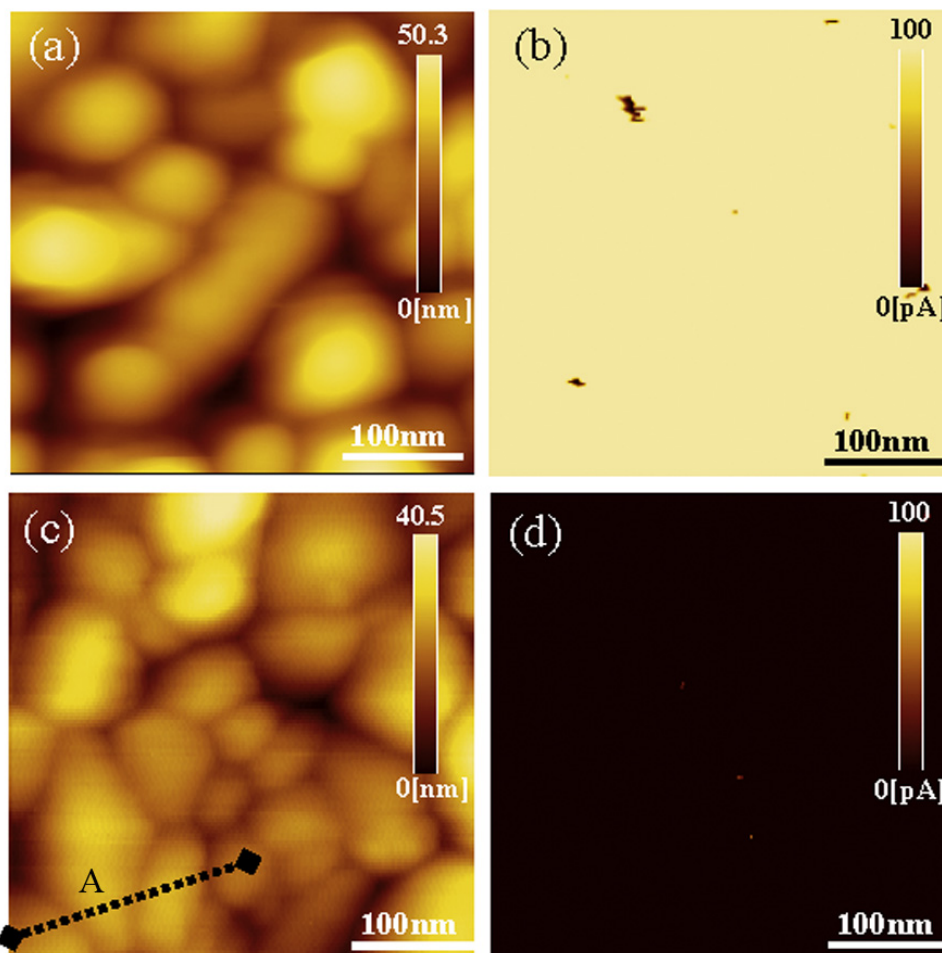


Figure 2. Topography of the S-1 sample (a) and corresponding current image (b). Topography of the S-2 sample (c) and corresponding current image (d). The tip bias during scanning is 0.5 V.

the GBS. This correlation between the current distribution and the topographic structure can be seen clearly by comparison of three linescans (see figure 3(g)), which are drawn at the same place in the topography of figure 2(c) and the current images of figures 3(c) and (d), respectively.

The resistance switching behaviors at the GS and GBS were studied by exerting the tip bias back and forth between 3 and -3 V. The I - V curves at both the GS and GBS of S-1 exhibited a good linear feature, indicating a good ohmic contact between the tip and the film, and no hysteresis (or resistance switching) can be observed (not shown). Figure 4(a) shows the I - V curves of a typical position at the GS of S-2. At the negative bias region, the current exhibited a sudden growth in the compliance current (100 pA) at a voltage of about -1.1 V in the bias ascending process whereas a decrease at a lower critical voltage, about -0.4 V, in the bias descending process. The resulting anticlockwise I - V hysteresis means a resistance change from the HRS to the LRS. In the case of reversed biases, the resistance switched back to the HRS again, as indicated by the occurrence of a clockwise I - V hysteresis. Repeating the I - V cycling, the resistance reversibly changed between the HRS and LRS, with a slight shift of the I - V curves to low bias. The spatial distribution of the switched sites can be described by the current mapping under a fixed tip bias.

The inset plot in figure 4(a) shows the current images obtained at the tip bias of -0.5 V. An obvious current bulge with the size of $\sim 10 \times 10$ nm² appeared after the negative voltage scanning, signifying the resistance reduction in this region. The tip size is ~ 25 nm in diameter, larger than the switched area. It is possible that the current flowed mainly through a part of the contact area between the tip and film due to the convex shape of the tip. This assumption is partially reflected by the higher lateral resolution in current images than in topography images. After the positive voltage sweeping, the main current bulge was erased although some residual current bulges (< 5 pA) can still be seen. Figure 4(b) shows the I - V curves of a typical position at the GBS of the S-2 sample. The I - V curves showed an obvious asymmetric behavior, which was consistent with the current image measurement (see figure 3). When reducing the tip bias, a shift of the I - V curve to the low bias always existed in the negative bias region, which might be caused by charging accumulation effects at the tip. No so-called reversible resistance switching can be observed. This conclusion was further confirmed by the local current mapping under the tip bias of -0.5 V after the negative voltage sweep (see the inset in figure 4(b)).

To evaluate the repeatability and reproducibility of the two resistance switching behaviors of the GS and GBS, a twofold

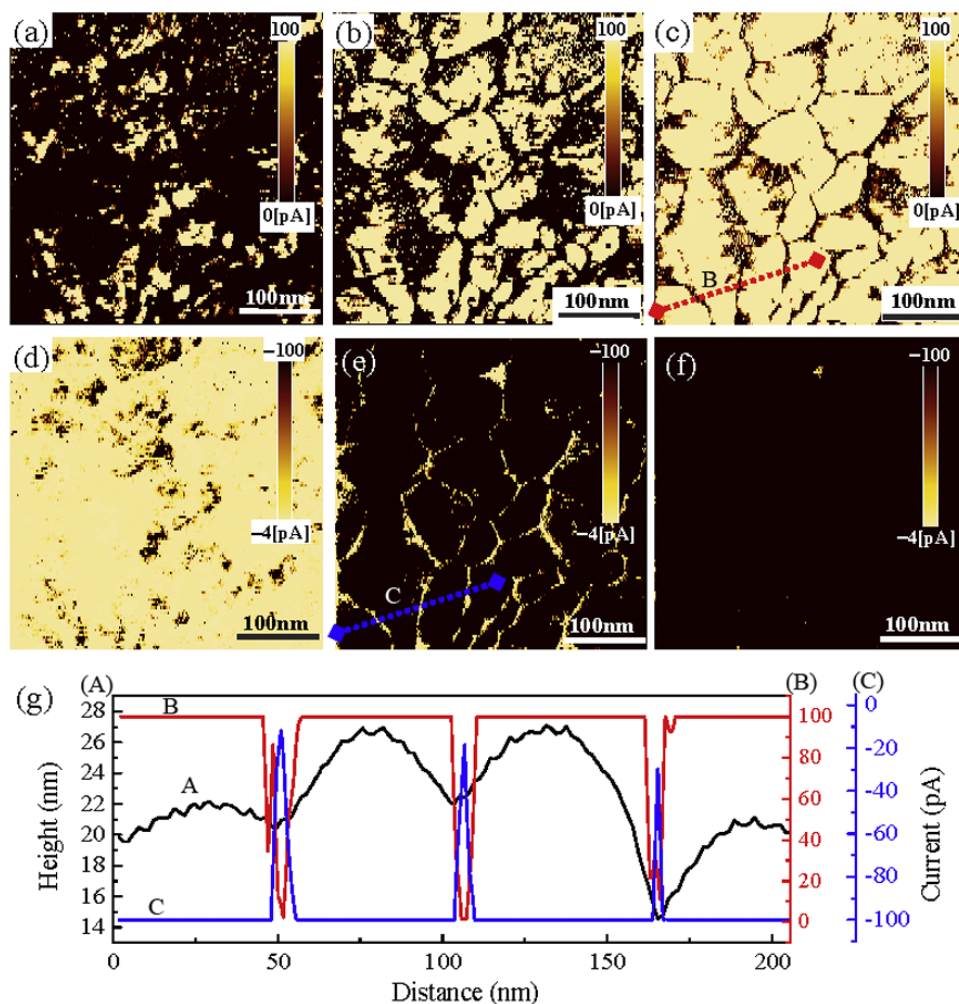


Figure 3. Current images of the S-2 sample with the tip bias of 1.0 V (a), 1.5 V (b), 2.0 V (c), 1.0 V (d), 1.5 V (e) and 2.0 V (f). All images correspond to the same area as figure 2(c). (g) Linescans of the current and topography at the position in part (c) (red line B), (e) (blue line C) and figure 2(c) (black line A).

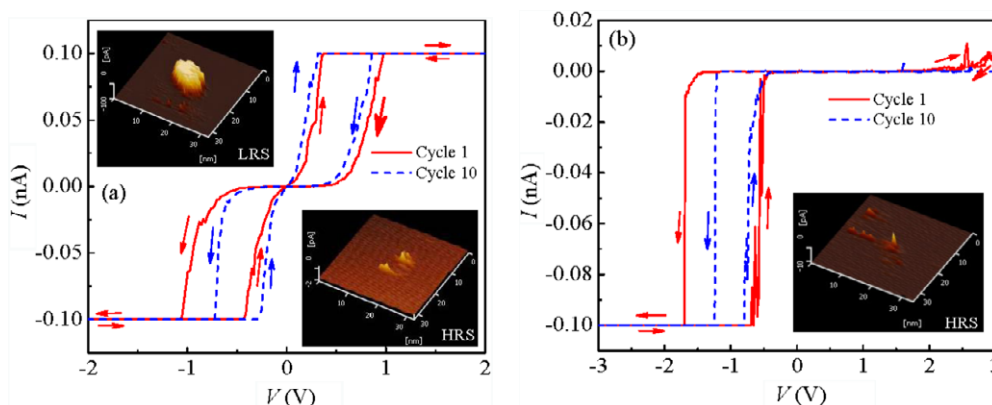


Figure 4. Local I - V characteristics at GS (a) and GBS (b) of the S-2 sample, measured by the CAFM tip with the external biases ranging from -3 to 3 V. The current compliance is 100 pA. Upper left and lower right insets in (a) show the current mappings after negative and positive voltage sweep, respectively. Inset in (b) shows the current mappings after negative voltage sweep. The current images were obtained under the tip bias of -0.5 V.

overwriting process, as explained below, was performed. First, a $0.6 \times 0.6 \mu\text{m}^2$ area in the center of a $1 \times 1 \mu\text{m}^2$ area was scanned under a tip bias of -3 V. Then a smaller inner area ($0.3 \times 0.3 \mu\text{m}^2$) with the same center as the previous image

was scanned under a tip bias of $+3$ V. The bright contrast in figure 5(b) indicates the LRS of the film resistance within the square image and the HRS outside. However, the current image of the LRS here is different from that of S-1 (see figure 2(b)),

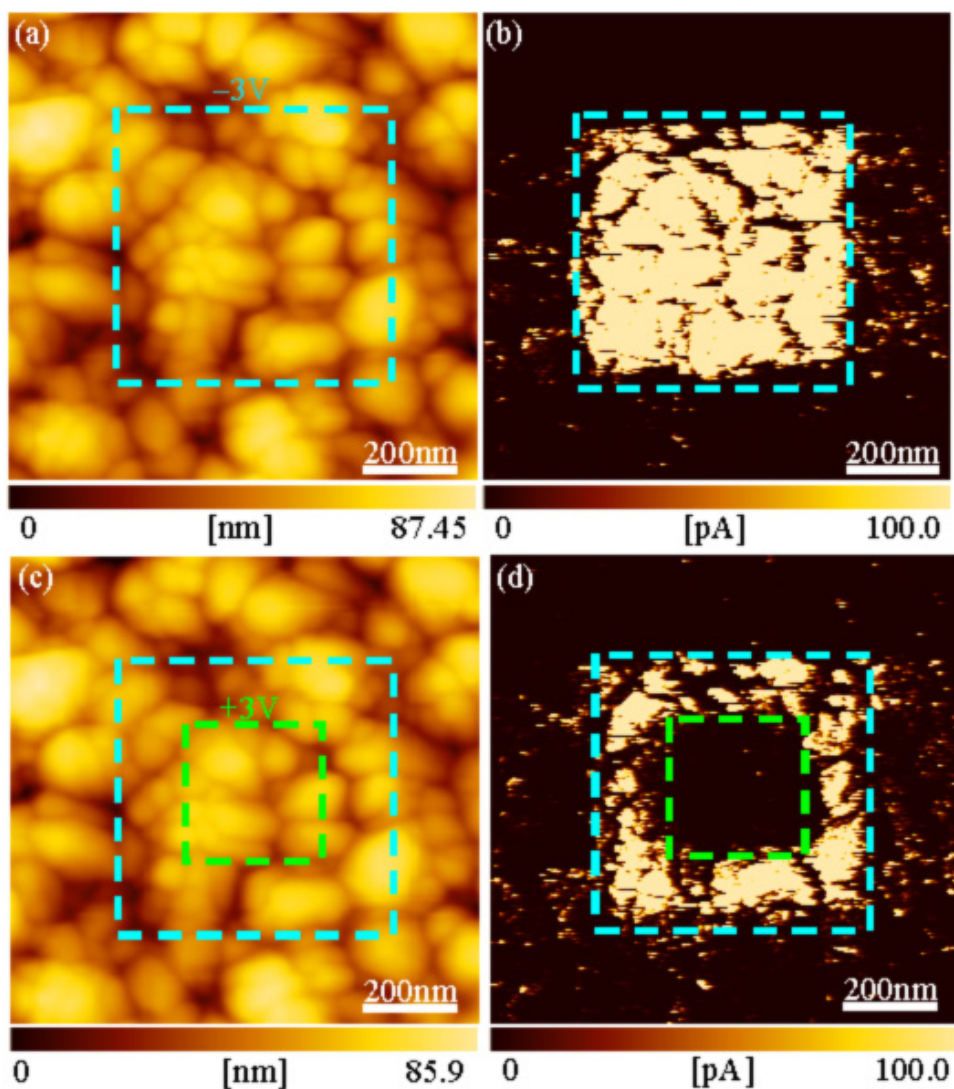


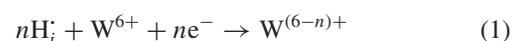
Figure 5. Topographies (left side) and the corresponding current images (right side) of the S-2 sample after sequential overwriting processes. The scattered spots in the dark region should be the artifacts due to a capacitance effect induced by the preamplifier. The current images were obtained under the tip bias of -0.5 V.

as shown by the presence of dark fragments along the GBS in the bright area. This further verifies no resistance change occurred at the GBS. After the scanning under a reverse bias ($+3$ V), the inner part of the bright area switched to dark (HRS) again (see figure 5(d)), indicating the reversibility of the resistance switching at the GS. We also carried out the current mapping in a vacuum environment ($<10^{-3}$ Pa) and obtained similar results, which indicates the unimportance of surface contamination of the sample and the external environments.

Up to now, the resistance switching mechanism in transition-metal oxides is still unclear, although many models have been proposed [24–27]. Recently, Waser *et al* overviewed the resistance switching phenomena in metal oxides based on electrochemical redox reactions and classified them into electrochemical metallization, valence changes and thermochemical mechanisms according to the dominant contribution [28]. In the present experiments, since no change of the surface topography can be observed during the resistance switching at the GS of tungsten oxide films, the

electrode diffusion into the film as well as the electrochemical metallization of the film with the external voltage can be excluded. Moreover, the polarity-dependent resistance switching excludes the dominant role played by the thermal effect even if it probably exists. Therefore, the local resistance switching at the GS of tungsten oxide films is suggested to be related to the valence change of tungsten ions.

One possible reason for the valence change of tungsten ions is electrochemical migration of protons under the electric field. Protons could be originated from the adsorption water, which hydroxylated tungsten ions to form W–O–H bands at the film surface. In this process, the following electrochemical reaction should be taken into consideration:



where H_i denotes a proton. As shown in figure 6, when the negative bias was applied between the film and the tip, protons would be injected into the film and then migrated to the cathode

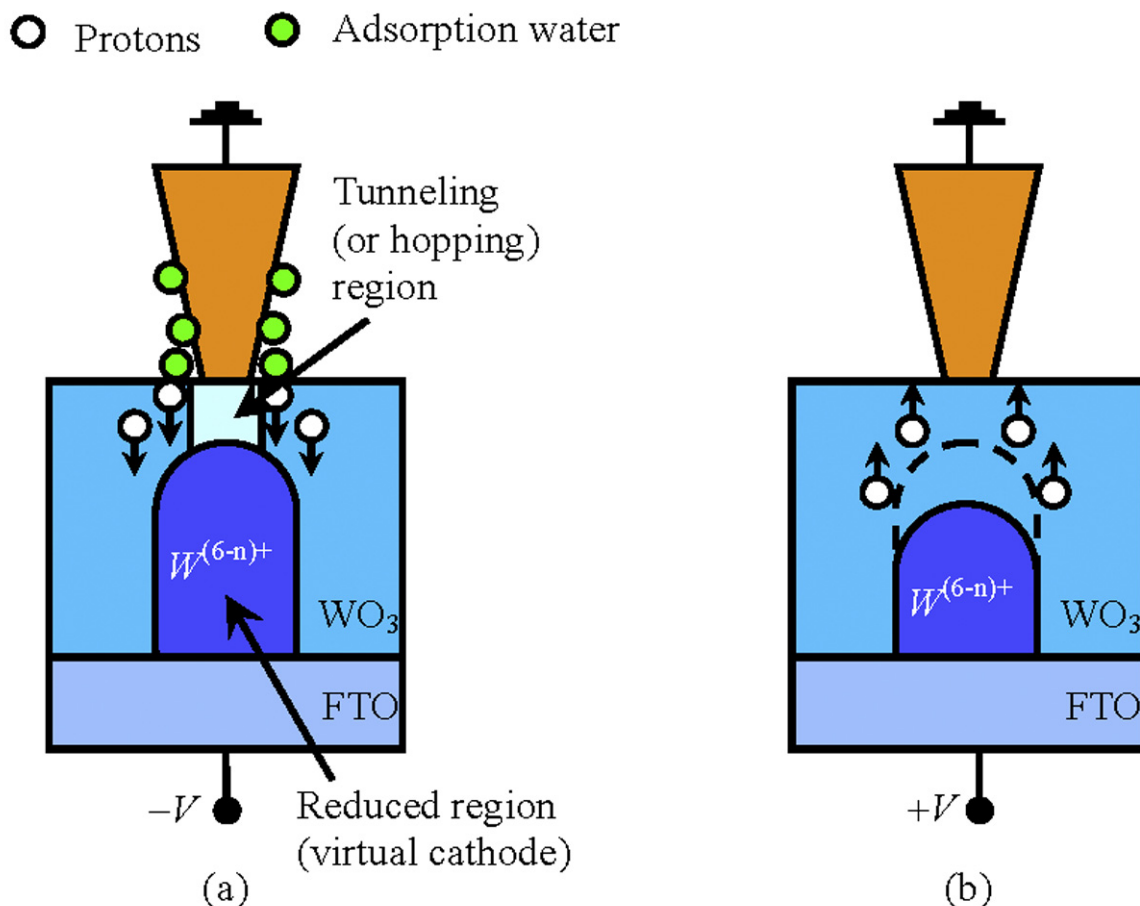


Figure 6. Schematic sketches of the mechanism for the resistance switching at the grain surfaces of tungsten oxide films. (a) and (b) represent the LRS and HRS, respectively.

and reduced the tungsten ions there. The reduced tungsten ions and the protons can form a metallic phase, which play a role of a virtual cathode. With the bias increasing, the reduced area grew longer and the electric field in the remaining part of the film increased. When the electric field reached the level to drive electrons tunneling (or hopping) through the remaining part of the film, the current increased greatly resulting in the nonlinear character of the I - V curves, as shown in figure 4(a). The reduced area was maintained by decreasing the voltage. Consequently, electrons can tunnel (or hop) through the film in the lower bias region, meaning the site above the reduced area becomes LRS (see figure 6(a)). At the high reverse bias, protons migrated towards the tip and reacted with oxygen to form W-O-H bonds at the film surfaces. Then the tungsten ions near the top region of the reduced area (encircled by a dashed line in figure 6(b)) were re-oxidized. This results in the increase of the electron tunneling (or hopping) distance and then the electron tunneling (or hopping) process under the lower bias was weakened (see figure 6(b)). Therefore, this site was restored to the HRS.

Another possible reason for the valence change of tungsten ions is electrochemical migration of oxygen vacancies. Compared with oxygen vacancies, protons should be easier to be driven by an electric field due to their lower

radius than oxygen ions. The two migration processes cannot be differentiated in our experiments. To completely understand the resistance switching mechanism, further detailed studies are still needed.

The different resistance switching property between the GS and GBS might be due to the lower density of oxygen vacancies at the GBS. That should be caused by the more preferential combination of oxygen with oxygen vacancies along the grain boundaries during the annealing process, which would be expected to form an oxygen-rich region at the GBS [29]. Consequently, the conductivity at the GBS was lower than the GS as well as the film bulk. As the electric field was applied, the voltage drop was mainly produced at the surface layer of the film, resulting in that the electric field in the bulk was not enough to drive the migration of protons or oxygen vacancies. Therefore, the resistance switching was suppressed.

4. Conclusion

In summary, we have investigated the electric property of two kinds of polycrystalline tungsten oxide films through CAFM measurement. The S-2 samples (oxygen-annealed) show a more insulative property than S-1 (as-prepared). For

S-2, we have demonstrated the different conductivity between the GS (grain surfaces) and GBS (grain boundary surfaces). Reversible resistance switching behavior only occurred at the GS of S-2 and the switching behavior was described by the local valence change of tungsten ions induced by electrochemical migration of protons or oxygen vacancies, which resulted in electron tunneling through the films under the lower bias. The different conductivity and resistance switching behavior between the GS and GBS were attributed to the different oxygen vacancy density caused by the post-annealing process. The present results would be especially meaningful for the fabrication of nanoscale resistive nonvolatile memory devices.

Acknowledgments

This work has been supported by the National Basic Research of China, the National Natural Science Foundation of China, the Knowledge Innovation Project of the Chinese Academy of Science and the Beijing Municipal Nature Science Foundation.

References

- [1] Liu S Q, Wu N J and Ignatiev A 2000 *Appl. Phys. Lett.* **76** 2749–51
- [2] Beck A, Bednorz J G, Gerber Ch, Rossel C and Widmer D 2000 *Appl. Phys. Lett.* **77** 139–41
- [3] Oligschlaeger R, Waser R, Meyer R, Karthäuser S and Dittmann R 2006 *Appl. Phys. Lett.* **88** 042901
- [4] Seo S *et al* 2004 *Appl. Phys. Lett.* **85** 5655–7
- [5] Rohde C, Choi B J, Jeong D S, Choi S, Zhao J S and Hwang C S 2005 *Appl. Phys. Lett.* **86** 262907
- [6] Chang W Y, Lai Y C, Wu T B, Wang S F, Chen F C and Tsai N J 2008 *Appl. Phys. Lett.* **92** 022110
- [7] Dong R *et al* 2007 *Appl. Phys. Lett.* **90** 042107
- [8] Sakamoto T, Sunamura H, Kawaura H, Hasegawa T, Nakayama T and Aono M 2003 *Appl. Phys. Lett.* **82** 3032–4
- [9] Schindler C, Puther Thermadam S C, Waser R and Koziicki M N 2007 *IEEE Trans. Electron Devices* **54** 2762–8
- [10] Koziicki M N, Park M and Mitkova M 2005 *IEEE Trans. Nanotechnol.* **4** 331–8
- [11] Chen X, Wu N J, Strozier J and Ignatiev A 2006 *Appl. Phys. Lett.* **89** 063507
- [12] Szot K, Speier W, Bihlmayer G and Waser R 2006 *Nat. Mater.* **5** 312–20
- [13] Szot K, Dittmann R, Speier W and Waser R 2007 *Phys. Status Solidi (RRL)* **1** R86–8
- [14] Lee M J *et al* 2009 *Nano Lett.* **9** 1476–81
- [15] Son J Y and Shin Y H 2008 *Appl. Phys. Lett.* **92** 222106
- [16] Yoshida C, Kinoshita K, Yamasaki T and Sugiyama Y 2008 *Appl. Phys. Lett.* **93** 042106
- [17] Muenstermann R, Dittmann R, Szot K, Mi S, Jia C L, Meuffels P and Waser R 2008 *Appl. Phys. Lett.* **93** 023110
- [18] Yang L, Kuegeler C, Szot K, Ruediger A and Waser R 2009 *Appl. Phys. Lett.* **95** 013109
- [19] Goux L, Polspoel W, Lisoni J G, Chen Y Y, Pantisano L, Wang X P, Vandervorst W, Jurczak M and Wouters D J 2010 *J. Electrochem. Soc.* **157** G187–92
- [20] Himpfel F J, Morar J F, McFeely F R and Pollak R A 1984 *Phys. Rev. B* **30** 7236–41
- [21] Fleisch T H and Mains G J 1982 *J. Chem. Phys.* **76** 780–6
- [22] Santucci S, Lozzi L, Maccallini E, Passacantando M, Ottaviano L and Cantalini C 2001 *J. Vac. Sci. Technol. A* **19** 1467–73
- [23] Gillet M, Lemire C, Gillet E and Aguir K 2003 *Surf. Sci.* **532–535** 519–25
- [24] Waser R and Aono M 2008 *Nat. Mater.* **6** 833–40
- [25] Sawa A 2008 *Mater. Today* **11** 28–36
- [26] Yang J J, Pickett M D, Li X, Ohlberg D A A, Stewart D R and Williams R S 2008 *Nat. Nanotechnol.* **3** 429–33
- [27] Chang S H, Lee J S, Chae S C, Lee S B, Liu C, Kahng B, Kim D W and Noh T W 2009 *Phys. Rev. Lett.* **102** 026801
- [28] Waser R, Dittmann R, Staikov G and Szot K 2009 *Adv. Mater.* **21** 2632–63
- [29] Ramzan M and Brydson R 2005 *Sensors Actuators A* **118** 322–31